ICAS 2016
30th Congress of the International Council of the Aeronautical Sciences
DCC, Daejeon, Korea ; September 25-30, 2016

NUMERICAL SIMULATION OF AEROTHERMODYNAMIC CHARACTERISTICS OF FLOW OVER SPACE VEHICLE MODEL

Ivan Egorov*, Natalia Palchekovskaya *
*** Central Aerohydrodynamic Institute**

Keywords: *numerical simulation, hypersonic flow, space vehicle*

Abstract

In this work numerical simulation of flow over Martian space probe at wind tunnel conditions, corresponding to Mach numbers M = 7.5, 10. 5 and 14 for various angles of attack is carried out on basis of Navier-Stokes equations, which are solved using in-house software package HSFlow with possibility of distributed computing on multiprocessor computer. Peculiarities in behavior of aerodynamic and thermal characteristics of flow are discussed.

1 Introduction

Projects on exploration of Solar system planets and development of re-entry vehicles are of special interest in present time. Considerable part of these projects is related to experimental and theoretical studies for development of space vehicles for Mars investigation. Currently theoretical and experimental studies, related to investigation and development of Mars, are carried out. One of the guidelines of this research is the development of space probes for various applications. Usually they represent strongly blunted axisymmetrical bodies, contour of which in meridional section is constructed from segments of elementary curves. The best known among them are space probes Mars Pathfinder (American project) and Martian Sample Return Orbiter (MSRO) (European project). Both space probes are axisymmetrical blunted bodies, frontal surface of which has shape of a blunted circular cone with a wide half-angle, value of which close to the maximum one. They differ from each other by shape of the afterbody. In the first case it is constructed in the form of a blunted inverse cone, and in the second case – in the form of a circular cylinder of a finite length. Thus, it is convenient to divide space probes into two groups – a space probe type of Mars Pathfinder and a space probe type of MSRO. Space probes of the first type provide greater volume for arrangement of bulky useful load, but they have difficulties with thermal protection. Space probes of the second type are characterized by developed global zone of the detached flow, where the container with useful load is fully located.

Aerodynamic characteristics and aerodynamic heating of a space probe during its motion in the planet atmosphere can be determined by equations of viscous gas dynamics.

Progress in computational aerodynamics allows developing effective software packages for numerical analysis of unsteady three-dimensional Navier-Stokes equations. This makes it possible to carry out calculations for conditions of aerodynamic experiment.

2 Numerical method

In this work hypersonic flow over descent vehicle model is simulated on basis of 3D Navier-Stokes equations at free stream conditions, corresponding to experimental parameters in wind tunnel T-117 of TsAGI. In general case, within the framework of mechanics of continua, motion of fluid is described by three-dimensional unsteady Navier-Stokes equations, which are basis of direct numerical simulation of turbulent flow. Navier-Stokes equations in an arbitrary curvilinear frame of reference (ξ, η, ζ), where $x = x(\xi, \eta, \zeta)$, $y = y(\xi, \eta, \zeta)$, $z = z(\xi, \eta, \zeta)$ -

Cartesian coordinates, are written in divergent form:

$$\frac{\partial \mathbf{Q}}{\partial t}+\frac{\partial \mathbf{E}}{\partial \xi}+\frac{\partial \mathbf{G}}{\partial \eta}+\frac{\partial \mathbf{F}}{\partial \zeta}=\mathbf{0}$$

Here **Q** – vector of conservative dependent variables, **E**, **G**, **F** – flux vectors in curvilinear coordinate system. Vectors **E**, **G**, **F** are related to corresponding vectors $\mathbf{E}_c$, $\mathbf{G}_c$, $\mathbf{F}_c$ in Cartesian coordinate system by following formulas

$$\mathbf{Q}=J\mathbf{Q}_c,\ \mathbf{E}=J\left(\mathbf{E}_c\frac{\partial \xi}{\partial x}+\mathbf{G}_c\frac{\partial \xi}{\partial y}+\mathbf{F}_c\frac{\partial \xi}{\partial z}\right)$$

$$\mathbf{G}=J\left(\mathbf{E}_c\frac{\partial \eta}{\partial x}+\mathbf{G}_c\frac{\partial \eta}{\partial y}+\mathbf{F}_c\frac{\partial \eta}{\partial z}\right),$$

$$\mathbf{F}=J\left(\mathbf{E}_c\frac{\partial \zeta}{\partial x}+\mathbf{G}_c\frac{\partial \zeta}{\partial y}+\mathbf{F}_c\frac{\partial \zeta}{\partial z}\right),$$

where $J=\partial(x,y,z)/\partial(\xi,\eta,\zeta)$ - transformation Jacobian.

Curvilinear coordinate system (ξ, η, ζ) is applied for discretization on uniform grid. For this case given arbitrary computational grid in Cartesian coordinate system is mapped on uniform grid in curvilinear coordinate system.

Cartesian components of flux vectors $\mathbf{E}_c$, $\mathbf{G}_c$, $\mathbf{F}_c$ for three-dimensional Navier-Stokes equations are following

$$\mathbf{Q}_c=\begin{Vmatrix}\rho\\ \rho u\\ \rho v\\ \rho w\\ \rho e\end{Vmatrix},\ \mathbf{E}_c=\begin{Vmatrix}\rho u\\ \rho u^2+p+\tau_{xx}\\ \rho uv+\tau_{xy}\\ \rho uw+\tau_{xz}\\ \rho uH+I_x\end{Vmatrix},$$

$$\mathbf{G}_c=\begin{Vmatrix}\rho v\\ \rho uv+\tau_{xy}\\ \rho v^2+p+\tau_{yy}\\ \rho vw+\tau_{yz}\\ \rho vH+I_y\end{Vmatrix},\ \mathbf{F}_c=\begin{Vmatrix}\rho w\\ \rho wu+\tau_{xz}\\ \rho wv+\tau_{yz}\\ \rho w^2+p+\tau_{zz}\\ \rho wH+I_z\end{Vmatrix},$$

where ρ - density, u, v, w – Cartesian components of velocity vector **V**, $e=h-p/\rho+(u^2+v^2+w^2)/2$ - total energy per unit volume, $H=h+(u^2+v^2+w^2)/2$ - total enthalpy, $h=c_pT$ - static enthalpy; T - temperature, c_p -specific heat at constant pressure, **τ** - symmetric viscous stress tensor, related to strain velocity tensor **s** by linear relationship

$$\boldsymbol{\tau}=-\mu\mathbf{s}$$

Components of strain velocity tensor **s** for compressible gas are following

$$\mathbf{s}_{xx}=2\frac{\partial u}{\partial x}-\frac{2}{3}\mathrm{div}\mathbf{V},\quad \mathbf{s}_{yy}=2\frac{\partial v}{\partial y}-\frac{2}{3}\mathrm{div}\mathbf{V},$$

$$\mathbf{s}_{zz}=2\frac{\partial w}{\partial z}-\frac{2}{3}\mathrm{div}\mathbf{V},$$

$$\mathbf{s}_{xy}=\frac{\partial u}{\partial y}+\frac{\partial v}{\partial x},\quad \mathbf{s}_{xz}=\frac{\partial u}{\partial z}+\frac{\partial w}{\partial x},$$

$$\mathbf{s}_{yz}=\frac{\partial v}{\partial z}+\frac{\partial w}{\partial y},$$

and heat flux vector **I** is determined by expression

$$\mathbf{I}=-\lambda\mathrm{grad}(T)+\boldsymbol{\tau}\bullet\mathbf{V},$$

where μ and λ - coefficients of molecular viscosity and thermal conductivity.

Set of Navier-Stokes equations is closed by equation of state and by relationships between transport coefficients and pressure and temperature, form of which depends on the model of moving fluid. In this work perfect gas model is applied with equation of state

$$p=\rho RT/M$$

where R – universal gas constant, M – gas molar weight; molecular viscosity coefficient depends on temperature according to Sutherland law

$$\frac{\mu}{\mu_\infty}=\frac{1+\frac{T_\mu}{T_\infty}}{\frac{T}{T_\infty}+\frac{T_\mu}{T_\infty}}\left(\frac{T}{T_\infty}\right)^{\frac{3}{2}},$$

where T_μ = 110.4 K for air; Prandtl number $\mathrm{Pr}=\mu c_p/\lambda$ is constant.

In dimensionless Navier-Stokes equations Cartesian coordinates are divided by characteristic linear size L, time is divided by characteristic time L / V_∞, $t = \bar{t}L / V_\infty$, velocity components are divided by absolute value of free stream velocity vector V_∞, pressure is divided by double dynamic pressure $p = \bar{p}(\rho_\infty V_\infty^2)$, other gas dynamic variables are divided by their values in free stream. Described form of Navier-Stokes equations is used in numerical integration. Initial-boundary problem, formulated above, is solved numerically on basis of finite-volume method. It allows obtaining difference analogues of conservation laws:

$$\frac{\mathbf{Q}_{i,j,k}^{n+1}-\mathbf{Q}_{i,j,k}^{n}}{\Delta t}+\frac{\mathbf{E}_{i+1/2,j,k}^{n+1}-\mathbf{E}_{i-1/2,j,k}^{n+1}}{h_\xi}+\frac{\mathbf{G}_{i,j+1/2,k}^{n+1}-\mathbf{G}_{i,j-1/2,k}^{n+1}}{h_\eta}+$$
$$+\frac{\mathbf{F}_{i,j,k+1/2}^{n+1}-\mathbf{F}_{i,j,k-1/2}^{n+1}}{h_\zeta}=0$$

where n – the number of time layer; Δt – value of time step; i, j, k and h_ξ, h_η, h_ζ – node numbers and ξ, η, ζ steps correspondingly.

For monotone difference scheme flux calculation in half-integer nodes is carried out on basis of Riemann problem solution. This problem comes to solution of nonlinear set of algebraic equations.

For approximation of convective component of flux vectors **E**, **G**, **F** in half-integer nodes monotone Godunov scheme [1] and approximate Roe technique for Riemann problem solution are used.

To increase approximation order for interpolation of dependent variables on edge of elementary cell minimum derivatives principle (MUSCL) [2 - 4] is used:

$$\mathbf{Q_L}=\mathbf{Q}_i+\frac{1}{2}m\left(\mathbf{Q}_i-\mathbf{Q}_{i-1},\mathbf{Q}_{i+1}-\mathbf{Q}_i\right)$$

$$\mathbf{Q_R}=\mathbf{Q}_i-\frac{1}{2}m\left(\mathbf{Q}_{i+1}-\mathbf{Q}_i,\mathbf{Q}_{i+2}-\mathbf{Q}_{i+1}\right)$$

and function $m(a,b)$ is following:

$$m(a,b)=\begin{cases}a, & ab>0, \quad |a|<|b|\\ b, & ab>0, \quad |a|>|b|\\ 0, & ab\le 0\end{cases}$$

For approximation of diffusive component of flux vectors **E**, **G** and **F** on the edge of elementary cell central difference scheme of second order accuracy is applied.

Calculations are fulfilled for perfect gas using in-house software package HSFlow.

3 The problem statement

Hypersonic flow over space probe model is simulated numerically for three regimes (Table 1).

No.	M_∞	Re_1, m^{-1}	T_∞, K
1	7.5	4.284×10^6	62.6
2	10.5	2.770×10^6	66.42
3	14	0.836×10^6	49.8

The problem is solved in three-dimensional statement, two-dimensional grid is rotated 180 degrees about the symmetry line in order to obtain three-dimensional computational grid (Figure 1). On the solid surface no-slip boundary condition (u = 0) and isothermal condition (T_w = 300 K) are set. On the outer boundary of the computational domain free stream boundary condition set (in the front part of the body) or variables extrapolation from inside of domain is applied (in the rear part of the body) [5, 6]. On the boundary of computational domain, coinciding with symmetry plane y = 0, symmetry boundary condition is set. On the degenerate boundaries extrapolation boundary condition is set. Free stream conditions are used as initial approximation.

Computational grids with 5×10^5, 4×10^6 and 32×10^6 nodes are used for simulation. Near the solid surface grid clustering is made in order to resolve boundary layer. Grids are splitted on blocks (24 and 96) along longitudinal and transversal coordinates in order to fulfill parallel calculations using multiprocessor super computers.

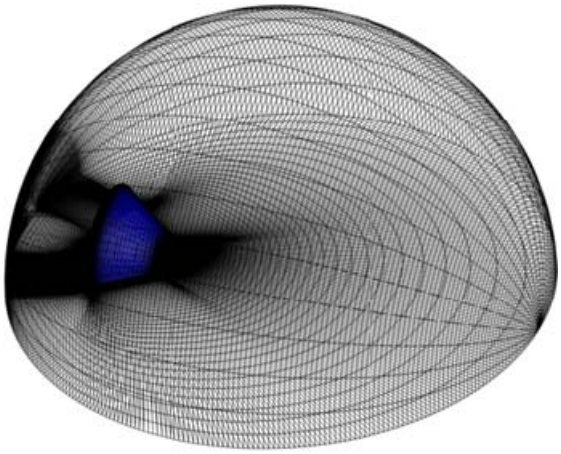

Fig. 1. Computational grid for three-dimensional grid

4 Results of numerical simulation

Analysis of results is carried out taking into account all given test regimes in the wind tunnel. In Figure 2 to Figure 4 Mach number fields with streamlines for three angles of attack 0°, 10°, 25° at free stream Mach number 7.5 are given. These fields show how the flow behavior changes depending on angle of attack. It can be seen, that rear separation zone shifts closer to leeward side of the vehicle as angle of attack increases.

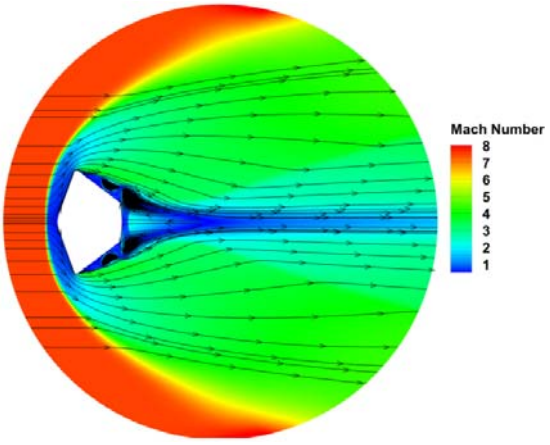

Fig. 2. Mach number field at angle of attack 0°

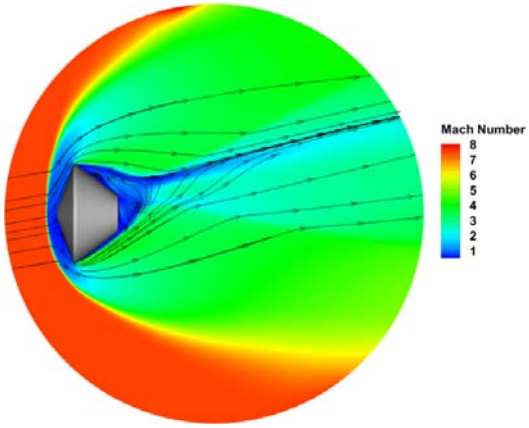

Fig. 3. Mach number field at angle of attack 10°

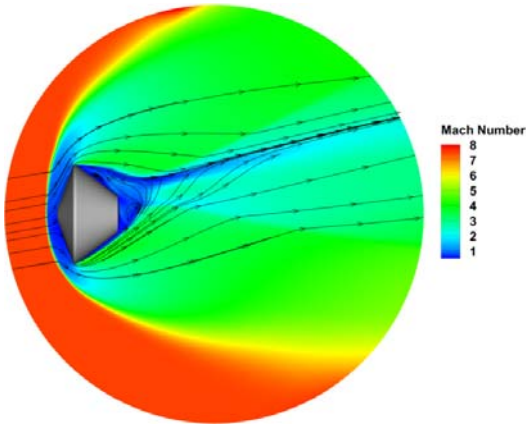

Fig. 4. Mach number field at angle of attack 25°

In Figure 5 to Figure 7 distributions of pressure coefficient along y coordinate for three angles of attack at fixed Mach number are presented. As can be seen from given dependencies, angle of attack has a significant impact on behavior of pressure coefficient on the leeward surface. Nonmonotonic behavior of pressure coefficient results from shape of the vehicle surface, which has curvature discontinuity at point of spherical and conic parts conjuction.

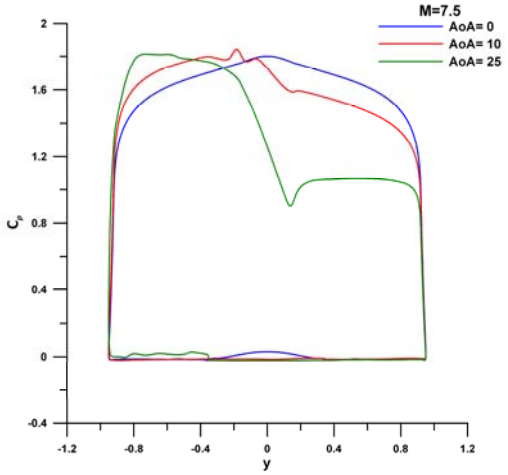

Fig. 5. Pressure coefficient distribution at $M_\infty = 7.5$

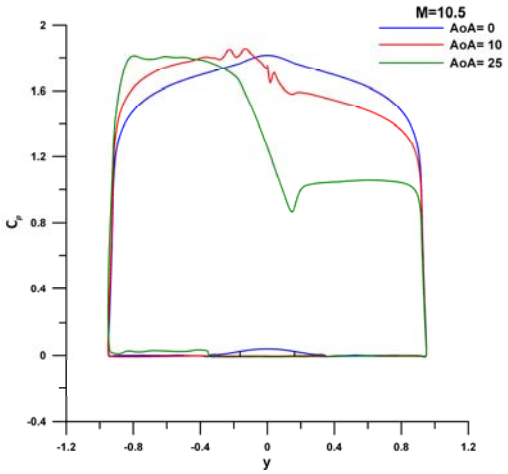

Fig. 6. Pressure coefficient distribution at $M_\infty = 10.5$

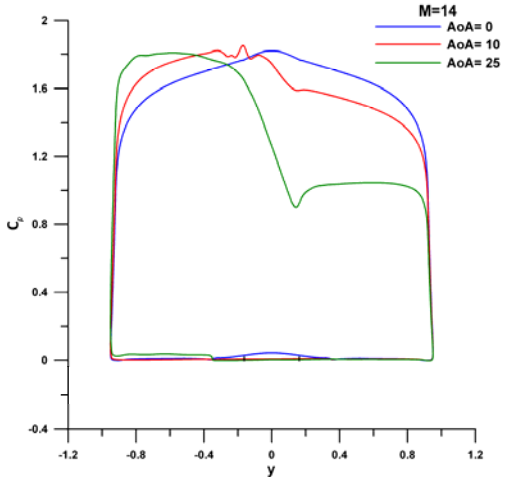

Fig. 7. Pressure coefficient distribution at $M_\infty = 14$

In Figure 8 to Figure 10 distributions of Stanton number are given for three angles of attack at fixed free stream Mach number, which characterizes heat flux on the body surface.

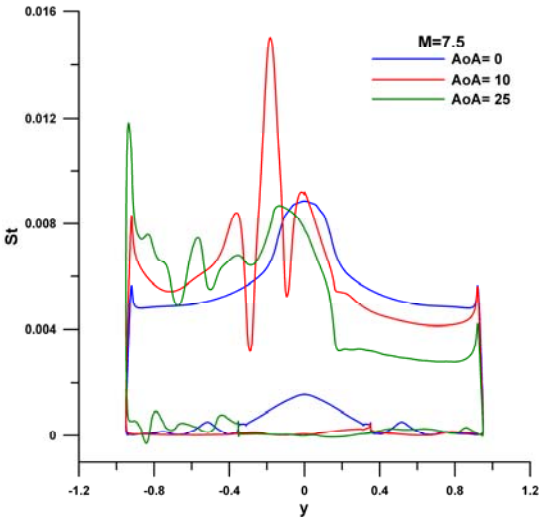

Fig. 8. Stanton number distribution at $M_\infty = 7.5$

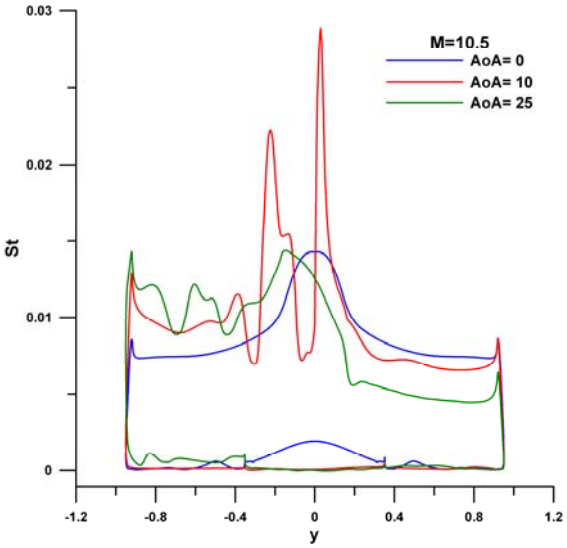

Fig. 9. Stanton number distribution at $M_\infty = 10.5$

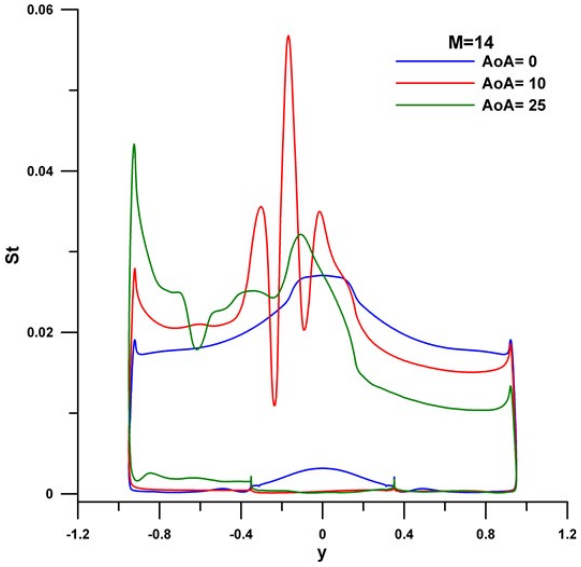

Fig. 10. Stanton number distribution at $M_\infty = 14$

It is seen that Stanton number distributions for each angle of attack have strong "peaks", which correspond to sharp heat flux increase near forward stagnation point. Nonmonotonic behavior of Stanton number near y values -0.18 and 0.18 on the frontal surface is related to, as for pressure coefficient, changes in the surface curvature. For all regimes under consideration the maximum value of Stanton number at angle of attack 10° substantially greater, than maximum values at other angles of attack. It is explained by the fact that location of spreading line is close to the point of the surface curvature discontinuity.

As noted above, calculations of this work are carried out for perfect gas model. But it is interesting to compare perfect gas results with results, obtained for other models of atmosphere, taking into account non-equilibrium physico-chemical processes [7]. In Figure 11 to Figure 13 pressure coefficient distributions are presented for Mach numbers M = 7.5, M = 10.5, M = 14. For each Mach number three curves are given, corresponding to perfect gas, Martian atmosphere and Earth atmosphere.

At Mach number $M_\infty = 10.5$ there is one more curve, corresponding to perfect gas at $\gamma = 1.18$. It can be noted that distribution of pressure coefficient for perfect gas at $\gamma = 1.4$ is close to distribution for Earth atmosphere, and distribution of pressure coefficient for perfect gas at $\gamma = 1.18$ quantitatively and qualitatively correspond to case of Martian atmosphere.

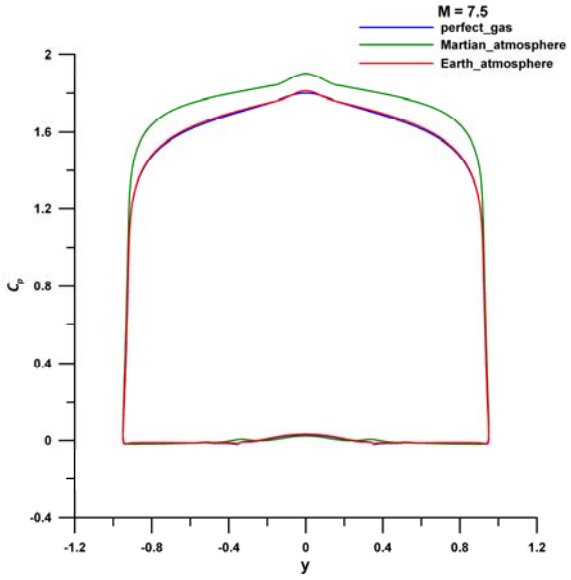

Fig. 11. Pressure coefficient distribution at $M_\infty = 7.5$ for different models of atmosphere

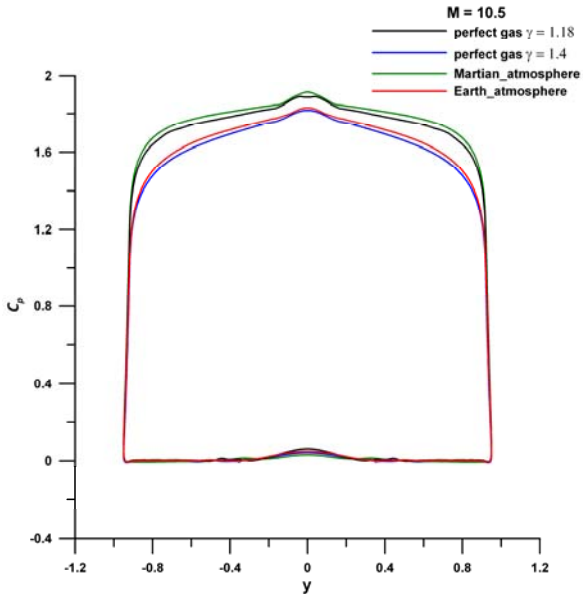

Fig. 12. Pressure coefficient distribution at $M_\infty = 10.5$ for different models of atmosphere

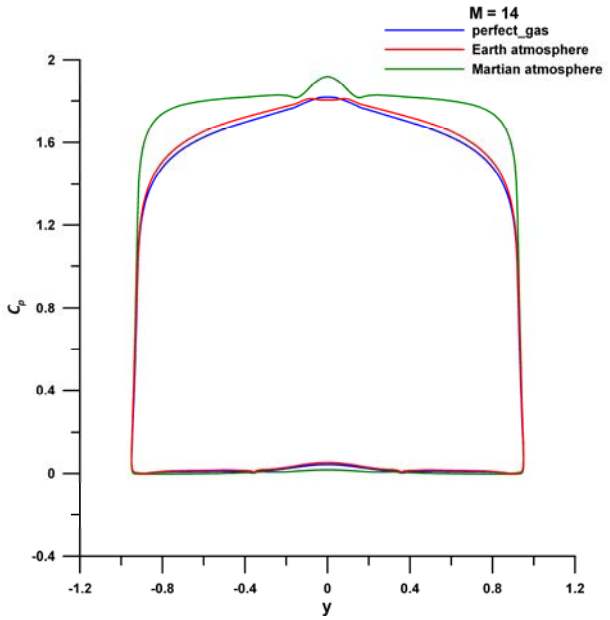

Fig. 13. Pressure coefficient distribution at $M_\infty = 14$ for different models of atmosphere

In Figure 14 distribution of Stanton number along y coordinate for three atmosphere models at Mach number $M_\infty = 7.5$ and zero angle of attack is given. It can be seen that taking into account real gas properties gives sufficient correction to flow characteristics.

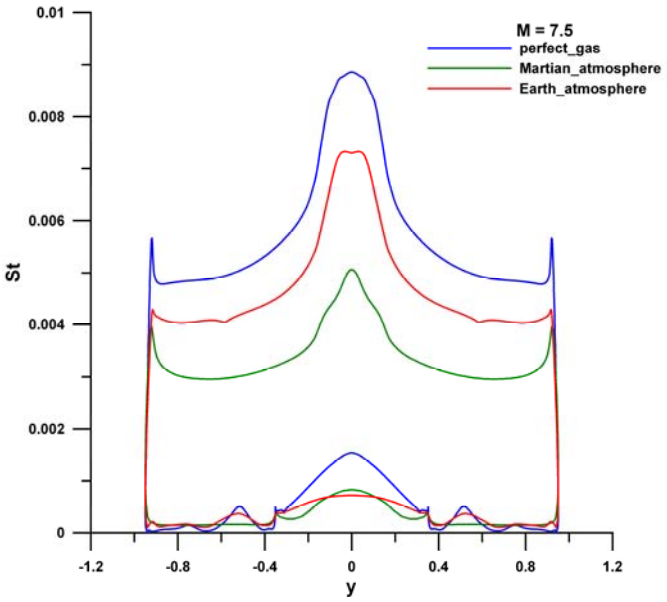

Fig. 14. Distribution of Stanton number for different atmosphere models

In Figure 15 comparison of experimental and numerical heat flux distributions is presented. The experiment is carried out by research group in TsAGI. The results have good quantitative agreement (difference of their maxima is about 15 percent). It can be seen that qualitatively these distributions are rather different. Namely, in numerical solution two local peaks are seen, which are absent in the experimental results. There are two possible causes of this difference: one is a low resolution in heat flux measurement technique, and another is some numerical effects, which result in sharply nonmonotonic behavior of heat flux.

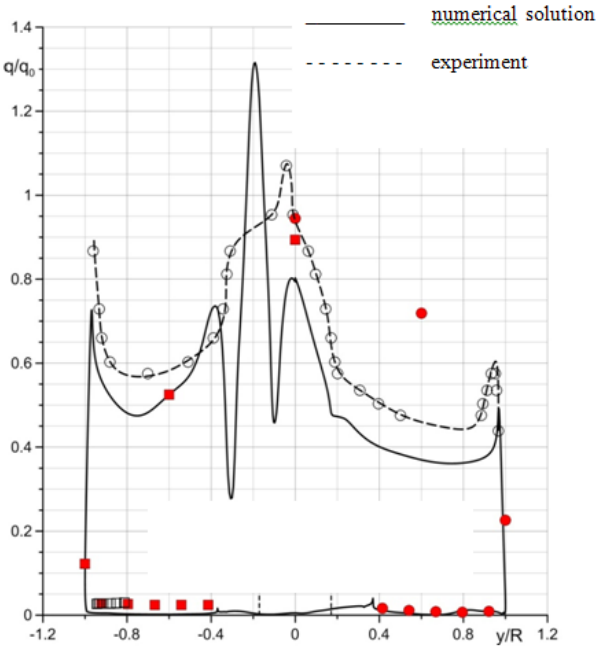

Fig. 15. Comparison of normalized heat flux distribution in numerical solution and experiment

5 Conclusions

On basis of numerical simulation analysis of Mach number and angle of attack influence on flow field structure and heat flux on the vehicle surface is fulfilled. It is showed that substantial heat flux increase is related to features of flow field in the vicinity of surface curvature discontinuity.

The reported study was funded by RFBR according to the research project No. 16-38-00274 мол_а.

References

[1] Godunov S.K. Finite-difference method for numerical computation of discontinuous solutions of the equations of fluid dynamics. *Mat. Sbornic*, Vol. 47, pp. 271- 306, 1959 (In Russian).

[2] Kolgan V. P. Application of the minimum-derivative principle in the construction of finite-difference schemes for numerical analysis of discontinuous solutions in gas dynamics. *Uchenye Zapiski TsAGI*, Vol. 3, No. 6, pp. 68 – 77, 1972 (In Russian).

[3] Saad Y., Shultz M.H. GMRes: a generalized minimal residual algorithm for solving nonsymmetric linear systems. *SIAM J. Scient. and Statist. Comp.*, Vol. 7, No. 3, pp. 856–869, 1986.

[4] Bashkin V.A, Egorov I.V. *Numerical simulation of the viscous perfect gas dynamics.* M.: Fizmatlit. 2012.

[5] Egorov I.V., Palchekovskaya N.V., and Shvedchenko V.V. The effect of spatial perturbations of a supersonic flow on heat flux to the surface of blunt bodies. *High Temperature*, Vol. 53, No. 5, pp. 713-726, 2015.

[6] Bashkin V. A., Egorov I. V., and Palchekovskaya N. V. The interaction of shock waves with a boundary layer on a sharp plate and a blunted plate. *High Temperature*, Vol. 54, No. 3, pp. 379 – 392, 2016.

[7] Egorov I., Pugach M. Numerical simulation of flow over descent vehicle for conditions of Martian atmosphere taking into account non-equilibrium physico-chemical processes. *Proceedings of 58th scientific conference of MIPT*. 2015. http://conf58.mipt.ru/static/reports_pdf/2013.pdf

Copyright Statement